energies

MDPI

Article

The Relevance of Lithium Salt Solvate Crystals in Superconcentrated Electrolytes in Lithium Batteries

Jake A. Klorman and Kah Chun Lau *

Department of Physics and Astronomy, California State University, Northridge, CA 91330, USA; jake.klorman.554@my.csun.edu

* Correspondence: kahchun.lau@csun.edu

Abstract: Based on the unique ubiquity of similar solvate structures found in solvate crystals and superconcentrated electrolytes, we performed a systematic study of four reported solvate crystals which consist of different lithium salts (i.e., LiMPSA, LiTFSI, LiDFOB, and LiBOB) solvated by acetonitrile (MeCN) based on first principles calculations. Based on the calculations, these solvate crystals are predicted to be electronic insulators and are expected to be similar to their insulating liquid counterpart (e.g., 4 M superconcentrated LiTFSI-MeCN electrolyte), which has been confirmed to be a promising electrolyte in lithium batteries. Although the MeCN molecule is highly unstable during the reduction process, it is found that the salt-MeCN solvate molecules (e.g., LiTFSI-$(MeCN)_2$, LiDFOB-$(MeCN)_2$) and their charged counterparts (anions and cations) are both thermodynamically and electrochemically stable, which can be confirmed by Raman vibrational modes through the unique characteristic variation in C≡N bond stretching of MeCN molecules. Therefore, in addition to the development of new solvents or lithium salts, we suggest it is possible to utilize the formation of superconcentrated electrolytes with improved electrochemical stability based on existing known compounds to facilitate the development of novel electrolyte design in advanced lithium batteries.

Keywords: batteries; salt–solvent solvates; superconcentrated electrolytes; redox potential; solvation science

Citation: Klorman, J.A.; Lau, K.C. The Relevance of Lithium Salt Solvate Crystals in Superconcentrated Electrolytes in Lithium Batteries. *Energies* **2023**, *16*, 3700. https://doi.org/10.3390/en16093700

Academic Editor: Haifeng Dai

Received: 2 April 2023
Revised: 15 April 2023
Accepted: 24 April 2023
Published: 26 April 2023

1. Introduction

Lithium salts are commonly known to dissolve in aprotic solvents, and the solvation properties of lithium metal cations in organic solutions have fascinated numerous researchers for many years due to their enormously important applications in the design and development of advanced Li-ion batteries [1,2]. To develop a robust, advanced Li-ion battery, an electrochemically stable and functional electrolyte that is highly tolerant to rapid, reversible anode/cathode reactions (without undergoing severe oxidative and reductive decomposition) is deemed necessary [3]. Among the common organic solvents, acetonitrile (MeCN) is one that is known to be oxidation tolerant. Because of its high dielectric constant ($\varepsilon \sim 35.69$) [4], many lithium salts can easily dissolve in MeCN solution and exhibit considerably high ionic conductivity. Despite these advantages, the use of MeCN in extensive Li-ion batteries remains limited due to its poor reductive stability, especially against lithium metal anodes [5].

To overcome this limitation, an electrochemically stable superconcentrated MeCN solution (i.e., ≥3–4 M) with enhanced reductive stability has recently been demonstrated [6,7]. According to Yamada et al. [7], a novel electrolyte that enables reversible lithium intercalation into a graphite electrode while successfully suppressing severe electrolyte decomposition and formation of lithium dendrites can be achieved when the lithium salt concentration in MeCN solution is increased over a certain threshold (~3 M). Compared with 1.0 M LiPF6/EC:DMC electrolyte, the reversible capacity decreases significantly with increasing rates. Whereas in contrast, the superconcentrated LiTFSI-MeCN electrolyte

exhibited much higher charging rate capability at all C-rates [7]. According to this finding [7], the origin of the enhanced reductive stability of the superconcentrated MeCN solution is attributed to the formation of unique networking solvate structures of Li^+ cations and bis(trifluoromethanesulfonyl)-imide ($TFSI^-$) anions with solvating MeCN solvents in solution, which leads to the formation of solvate ionic liquids-like systems (also called "solvent-in-salt" (SIS) systems) [8].

It is widely known that solvation structure and its formation are drastically different between dilute and concentrated solutions. Depending on the nature of the solvents and their capability of dissolving lithium salts, a wide range of salt concentrations, from ~3–5 M in nonaqueous media to ~4–10 M in aqueous media, are used [7,9]. At these high salt concentrations, significant ion pairing and aggregation occur, while the limited solvent molecules therein are largely bound to Li^+ cations, leading to entirely new salt–solvent solvate structures at both molecular and long-range scales, which may display various novel properties (e.g., transport, thermal, and interfacial) [7,9,10] that are important in Li-ion batteries. In contrast with dilute solutions (i.e., <1 M) [11], the unique aggregation state is observed in both superconcentrated solvate electrolytes and solvate crystals, which results in disordered aggregation of salt–solvent solvate structures in superconcentrated electrolytes as opposed to ordered aggregation of salt–solvent solvate structures which are found in solvate crystals [11,12].

When these lithium salts crystallize in the form of solvate crystals in an organic solvent (e.g., acetonitrile) solution, exploring their crystal structures, solvation shell, and physicochemical properties is beneficial for a basic understanding of the solvation science of lithium-ion-based electrolytes. Compared with that of lithium salts and organic solvents, a systematic study of lithium solvate crystals remains lacking at present, especially a study of the unique structure–property relationships at the molecular level. An in-depth understanding related to the variation in the ions speciation in electrolyte solution formed with various types of solvates and their distribution is important to help us to fine-tune their solvation structure and physicochemical properties for novel electrolyte design. Besides revealing an important insight into the unique salt–solvent solvation structure in both solvate crystals and superconcentrated solutions, this will help us identify a new avenue in the design of superconcentrated electrolytes, which is critical in the development of high-energy-density Li-ion batteries based on lithium metal anodes.

With this as motivation, we carried out a systematic study of four reported solvate crystals, which consist of different lithium salts solvated by MeCN solvent molecules in crystalline structures, based on first principles calculations. In this work, the basic properties of the signature salt-MeCN solvate structures were analyzed in terms of thermodynamic and electrochemical stability, chemical bonding, and electronic and vibrational properties based on density functional theory (DFT) calculations. With this as a baseline study, we hope to enhance the basic understanding of the fundamental properties of lithium salt–solvent solvate structures in solvate crystals, which, in turn, will help us to better understand the similar lithium salt-MeCN solvate features in superconcentrated MeCN-based electrolytes in high-energy-density Li battery applications.

2. Theoretical Methods

In this work, four different lithium salts, i.e., lithium bis(trifluoromethanesulfonyl)-imide, $LiN(SO_2CF_3)_2$ (LiTFSI); lithium (3-methoxypropyl)((trifluoromethyl)-sulfonyl)amide, $Li[CF_3SO_2N(CH_2)_3OCH_3]$ (LiMPSA); lithium difluoro(oxalate)borate, $LiBF_2(C_2O_4)$ (LiDFOB); and lithium bis(oxalate)borate, $Li[B(C_2O_4)_2]$ (LiBOB), which solvate MeCN solvents as solvate crystals, are considered. Specifically for these four lithium salts, LiMPSA and LiTFSI are N based, whereas LiDFOB and LiBOB are B based. For all the simulations, the initial simulation cells and configurations were based on the reported findings from experiments [13–16]. All the calculations of solvate crystals were performed in the framework of DFT using the Vienna Ab Initio Simulation Package (VASP) version 5.4.4 [17,18]. The projector-augmented wave (PAW) method [19] and the Perdew–Burke–Ernzerhof (PBE)

exchange-correlation functional [20] were used to describe the exchange–correlation effects. To include the influence of intermolecular interactions, Grimme's D3 correction term [21] was applied to include the van der Waals (vdW) interactions throughout the simulations. For all the calculations, the plane-wave kinetic energy cutoff was set to 500 eV. The energy convergence was set to 10^{-5} eV, and all the configurations were fully relaxed until the residual force on each atom was less than 0.01 eV/Å. For all these DFT calculations, a Γ-centered K-mesh with a density of no less than 2 points per Å (i.e., KSPACING = 0.5) was used to sample the Brillouin zone during the simulation cell relaxation and geometry optimization.

The optimized structures, especially the constituent lithium salt and MeCN molecules, obtained from VASP simulation were further interrogated for their electronic, thermochemical, and vibrational (i.e., Raman spectroscopy) properties by using the quantum chemistry method as implemented in the Gaussian 16 code [22]. The Becke three-parameter hybrid exchange functional combined with the LYP correlation (referred to as B3LYP) [23] and the 6–31 + G(d,p) basis set were employed in these calculations. In the geometry optimization procedure, the convergence criteria for gradient and energy were set to 10^{-4} hartree/Å and 10^{-9} hartree, respectively. The optimized configuration of neutral, anionic, and cationic states of MeCN and lithium salt (i.e., LiTFSI, LiMPSA, LiDFOB, and LiBOB), and their representative salt-MeCN solvate molecules were tested for electrochemical stability by computing their vibrational frequencies.

As an approximation, the electrochemical stability of MeCN, lithium salt, and salt-MeCN solvate molecules were quantified based on the free energy change for reduction or oxidation processes as follows [24]:

$$\text{oxidation potential, } E_{ox} = \frac{[\Delta G(S^+) - \Delta G(S)]}{F} - 1.24 \quad (1)$$

$$\text{reduction potential, } E_{red} = \frac{-[\Delta G(S^-) - \Delta G(S)]}{F} - 1.24 \quad (2)$$

where F is Faraday's constant; the free energy changes of neutral (s), anionic (s^-), and cationic (s^+) states are taken to be the sum of the free energy (ΔG) change in the gas phase since the change in electrons in energy from vacuum to the non-aqueous solution is negligibly small and would not change the qualitative trend of redox potentials [24,25]. Besides redox potentials, we also quantified the stability of charged species of MeCN, lithium salt molecules, and salt-MeCN solvate molecules based on adiabatic ionization potential ($IP = E(S^+) - E(S)$) and electron affinity ($EA = E(S) - E(S^-)$), where $E(S/S^-/S^+)$ is the total energy of neutral, anionic, and cationic species, respectively [26,27].

3. Results and Discussion

3.1. Structure Analysis

It is known that the crystalline salt–solvent solvate structures are generally obtained during the crystals' growth of salt in a given solvent. In this work, all these lithium salts are found to be highly soluble in MeCN solution, and the unique lithium salt-MeCN solvate structures are formed during the recrystallization process [28,29]. Detailed analysis of these thermodynamically stable salt-MeCN solvate structures is, therefore, necessary to help us understand the formation and unique structure–property relationship of the solvation shell of these electrolytes.

3.1.1. LiMPSA-MeCN Solvate Crystal

The solvate structure consists of lithium sulfonamide ($Li[CF_3SO_2N(CH_2)_3OCH_3]$, LiMPSA) salt, which is based on the (3-methoxypropyl)((trifluoromethyl)-sulfonyl)amide (MPSA) anion, and acetonitrile solvent molecules [13] (Figure 1). As reported recently [30,31], this family of MPSA salt features an unusual melting point trend, where the melting point of the salts decreases as the cation increases in size from lithium (Li) to potassium (K) [30]. Notably, KMPSA features an extremely low melting point of only ~51 °C, which could make

it a promising candidate of single cation ionic liquids (SCILs) [31]. In this work, LiMPSA-MeCN solvate crystal is a monoclinic cell, and it consists of 8 LiMPSA salt and 4 MeCN solvent molecules [13] with a cell density of ~1.51 g/cm^3 according to the DFT optimized cell lattices (Table S1). From the DFT calculation, the thermodynamic stability of this solvate crystal is found to be E_b ~ 3.68 eV/Li, which is modest among the rest (Table 1). According to our finding, the low binding energy of this solvate crystal might be attributed to the fact that not all the MeCN solvents are directly bonded by Li^+ ions within the inner solvation shell. However, it is noteworthy that solid structures with large empty channels or cavities are generally not stable [32], and the crystals may not be obtained if the intrinsically unstable scaffolding of salt or solute molecules is not supported by suitable solvent molecules. For the LiMPSA-MeCN solvate crystal, it was found that MeCN solvents' molecules are incorporated into the crystal lattices within the channels along the (010) direction approaching methyl groups of MPSA, which stabilize this solvate crystal. As shown in Figure 2, the tetracoordinated Li^+ is connected to a nitrogen atom (R_{Li-N} ~ 2.00 Å), sulfonyl oxygens (R_{Li-O} ~ 1.91 Å), and an ether oxygen (R_{Li-O} ~ 1.95 Å) of MPSA anions that render the inner solvation shell. According to Dillon et al. [13], the flexibility of the ether oxygen in the MPSA anion may facilitate Li^+ ionic conductivity, and this unique feature has been found in KMPSA-based SCILs in a recent study [31].

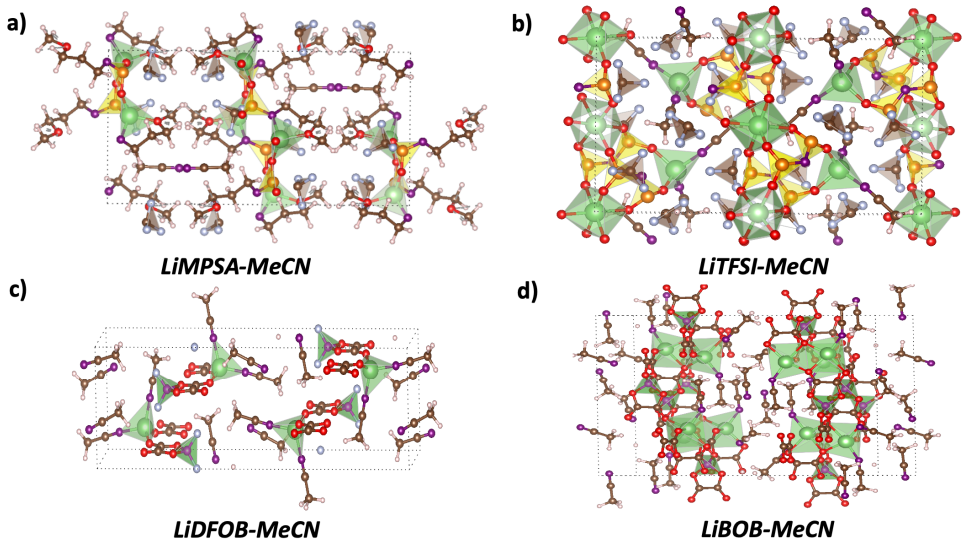

Figure 1. Crystalline solid of lithium salt-MeCN solvates considered in this study: (**a**) LiMPSA-MeCN, (**b**) LiTFSI-MeCN, (**c**) LiDFOB-MeCN, and (**d**) LiBOB-MeCN. The green polyhedral region is the highlighted region that shows the coordination of the Li^+ cation with the neighboring salt anion and the MeCN solvent molecules. Color of atoms: boron (pink), carbon (brown), fluorine (gray), hydrogen (white), lithium (green), nitrogen (purple), oxygen (red), and sulfur (orange).

Table 1. DFT-predicted binding energy, E_b (in eV/Li), and electronic band gap, E_g (in eV), of the several solvate crystals studied in this work.

System	Binding Energy, E_b (eV/Li)	Electronic Band Gap, E_g (eV)
LiMPSA-MeCN	3.68	5.65
LiTFSI-MeCN	2.52	6.72
LiDFOB-MeCN	3.90	3.75
LiBOB-MeCN	3.90	3.70

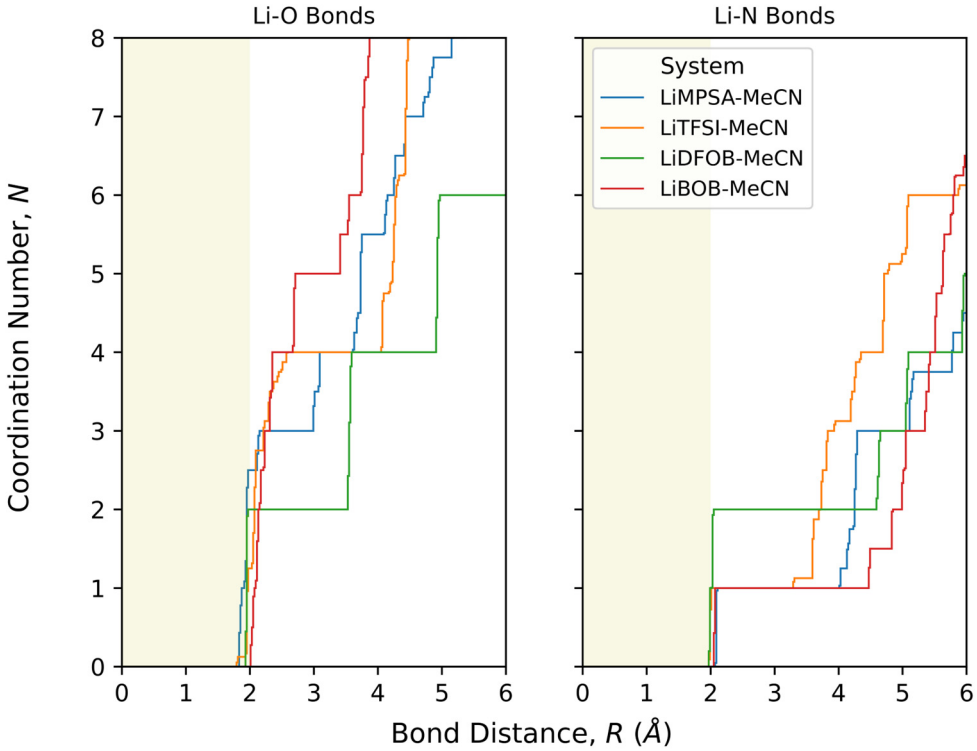

Figure 2. Coordination number, N, was determined by (**left**) Li-O and (**right**) Li-N bonds defined by Li^+ ions in the solvation shell of these solvate crystals. The yellow highlighted region shown is the approximate radial distance (R ~ 2.0 Å) for the inner solvation shell.

3.1.2. LiTFSI-MeCN Solvate Crystal

Similar to the LiMPSA-MeCN solvate crystal, the LiTFSI-MeCN solvate crystal cell is found to be monoclinic as was reported [14]. This solvate crystal consists of 8 LiTFSI salt and 8 MeCN solvent molecules [14] with a cell density of ~1.91 g/cm^3 according to DFT-optimized cell lattices (Table S1). For this solvate crystal (Figure 1), there are 2 types of Li^+ cations that reside in this solvate system: (1) A total of 6 coordinated Li^+ cations that bonded with the neighboring 6 oxygen ($R_{Li-O} \sim 2.1 - 2.2$ Å) atoms from bis(trifluoromethanesulfonyl)-imide (TFSI) anions, which relates to salt–salt interactions, and (2) a total of 4 coordinated Li^+ cations that bonded with the neighboring 2 O atoms from the TFSI anion ($R_{Li-O} \sim 1.95$ Å), as well as 2 N atoms from the MeCN solvent molecules ($R_{Li-N} \sim 2.00$ Å), which relate to salt–solvent interactions that render a stable, unique LiTFSI-$(MeCN)_2$ solvate complex in the lattice. Due to this unique interplay of salt–salt and salt–solvent interactions, this yields an average of five in the coordination number for Li^+ cations in the LiTFSI-MeCN solvate crystal dominated by Li-O and Li-N bonds separately in solvation shells within the bond distance of ~2.2 Å (Figure 2). For a LiTFSI-MeCN system, this chelate effect of the solvate complex is unique. For this binary component solvate system, the formation of two or more separate coordinate bonds between polydentate ligands and the central Li^+ ions are pronounced, and this led to a thermodynamically stable stoichiometric mixture of the salt–solvent solvate complex in the lattice with E_b ~ 2.52 eV/Li (Table 1). Interestingly, this unique feature (i.e., the LiTFSI-$(MeCN)_2$ solvation structure) is also found in ~4 M superconcentrated LiTFSI-MeCN electrolytes [7,11,33] applied in Li-ion and Li-S (lithium-sulfur) batteries.

3.1.3. LiDFOB-MeCN Solvate Crystal

For the LiDFOB-MeCN solvate crystal, it consists of four LiDFOB salt and twelve MeCN solvent molecules [15] in an orthorhombic lattice (Figure 1) with a cell density of ~1.41 g/cm^3 according to DFT-optimized cell lattices (Table S1). For this solvate system, not all MeCN solvent molecules are directly bonded with Li^+ cations or difluoro(oxalate)borate

($DFOB^-$) anions and form a solvation shell. For this unique LiDFOB-MeCN solvate system, the inner solvation shell is distributed equally by Li-O ($R_{Li-O} \sim 1.95$ Å) and Li-N bonds ($R_{Li-N} \sim 2.03$ Å), separately (Figure 2). Whereas for the rest of the uncoordinated MeCN solvent molecules, they are residing within the channels along the (001) direction of the crystal lattice, similar to the orientation found in MeCN molecular solids that are stabilized by relatively weak, long-range hydrogen bonds (Figure S1). From our observation, the MeCN solvent molecules in this system have essentially two ways to stabilize the LiDFOB-MeCN solvate system: (I) as ligands in completing the bond coordination around Li^+ ions in the inner solvation shell and (II) as space fillers to decrease the void space and/or lead to more efficient packing; this stabilizes the crystalline lattice with $E_b \sim 3.90$ eV/Li (Table 1), which is the most stable among the rest.

3.1.4. LiBOB-MeCN Solvate Crystal

Lithium bis(oxalate)borate, $Li[B(C_2O_4)_2]$ (LiBOB) salt has been proposed as an alternative lithium salt for the electrolyte in rechargeable Li-ion batteries that are free of explosive perchlorate, reactive fluoride, or toxic arsenic [16]. For the LiBOB-MeCN solvate crystal, the structure stability ($E_b \sim 3.90$ eV/Li) (Table 1) and its structural features are found to be similar to LiDFOB-MeCN. For this monoclinic crystal lattice, the structures contain two symmetrical independent LiBOB and five MeCN molecules [16]. It consists of 8 LiBOB salt and 20 MeCN solvent molecules with a cell density of ~1.51 g/cm^3 based on DFT-optimized cell lattices (Table S1). Similar to the LiDFOB-MeCN solvate system, there are two types of MeCN solvent molecules present in the crystalline lattice. For this system, the formation of the inner solvation shell (R ~2.2 Å) is attributed to the LiBOB salt–salt and LiBOB-MeCN salt–solvent interaction, which yields an average coordination number, $N \sim 5$, for Li^+ cations (Figures 1 and 2). For the inner solvation shell, it consists of four Li-O bonds ($R_{Li-O} \sim 2.05 - 2.20$ Å) from terminal oxygen atoms of the oxalate group of $[B(C_2O_4)_2]^-$ anions, and one Li-N bond ($R_{Li-N} \sim 2.05$ Å) with one MeCN ligand molecule (Figure 2). Whereas for the rest of the uncoordinated MeCN solvent molecules, they are stabilized within the channels along the (001) direction of the crystal lattice similar to the orientation found in the MeCN molecular solid that holds them together through relatively weak long-range C-H$\cdots$O and C-H$\cdots$N hydrogen bonds within the lattices (Figure 1).

3.2. Electronic Properties of Solvate Crystals

Similar to their constituent individual electronic insulating salt (i.e., LiMPSA, LiTFSI, LiDFOB, and LiBOB) and MeCN molecule (Figure S2), all these lithium salt-MeCN solvate crystals are found to be electronic insulators (Figure 3) with finite electronic band gaps that range from ~3.7–6.7 eV (Table 1), which is comparable to oxides (e.g., ZrO_2) [34] according to DFT prediction. Among these, the LiTFSI-MeCN solvate crystal is found to be the most insulating ($E_g \sim 6.7$ eV, Figure 3b), followed by LiMPSA-MeCN ($E_g \sim 5.7$ eV, Figure 3a), LiDFOB-MeCN ($E_g \sim 3.8$ eV, Figure 3c), and LiBOB-MeCN ($E_g \sim 3.8$ eV, Figure 3d). At the vicinity of the Fermi level (E_f), the electronic density of states (e-DOS) at the top valence band (TVB) of these solvate crystals are mostly dominated by the most electronegative elements (i.e., oxygen and nitrogen) of salt anions that bonded with Li^+ in the inner or first solvation shell of the salt-MeCN solvate structure, which helps to stabilize the crystalline lattice.

For the LiMPSA-MeCN solvate crystal, the unique electronic insulating feature is critical for this system to be used as an ionic conductor [13]. Whereas for the LiTFSI-MeCN solvate crystal, the electronic property ($E_g \sim 6.7$ eV) is found to be surprisingly similar to its insulating liquid counterpart, i.e., 4 M superconcentrated LiTFSI-MeCN electrolyte ($E_g \sim 4$ eV) [7], which confirmed that for a practical superconcentrated electrolyte in battery applications, the selected candidate has to be "electronic insulating" and "ionic conducting" [35–37]. Compared with the electronic charge distribution of the TVB of these solvate crystals, close proximity can be found with the highest occupied molecular orbital (HOMO) of the constituent salt-MeCN solvate structures, e.g., LiTFSI-$(MeCN)_2$ and

LiDFOB-$(MeCN)_2$, separately (Figure 4). In general, the distinctive electronic features of the molecular salt-MeCN solvate structure in these solvate crystals are found to be well preserved. Consistent with the e-DOS highlighted in Figure 3, both the electronic state of the TVB for the LiTFSI-MeCN solvate crystal and the HOMO for the LiTFSI-$(MeCN)_2$ solvate molecule are similar and are dominated by the TFSI anion oxygen atoms (Figure 4a). A similar trend is found in the LiDFOB-MeCN solvate crystal and the LiDFOB-$(MeCN)_2$ solvate molecule (Figure 4b), which suggests that these salt-MeCN solvate crystals are molecular solids; this is also the case for their counterparts in superconcentrated MeCN solution (e.g., 4 M superconcentrated LiTFSI-MeCN electrolyte) that have been applied in batteries [7,33].

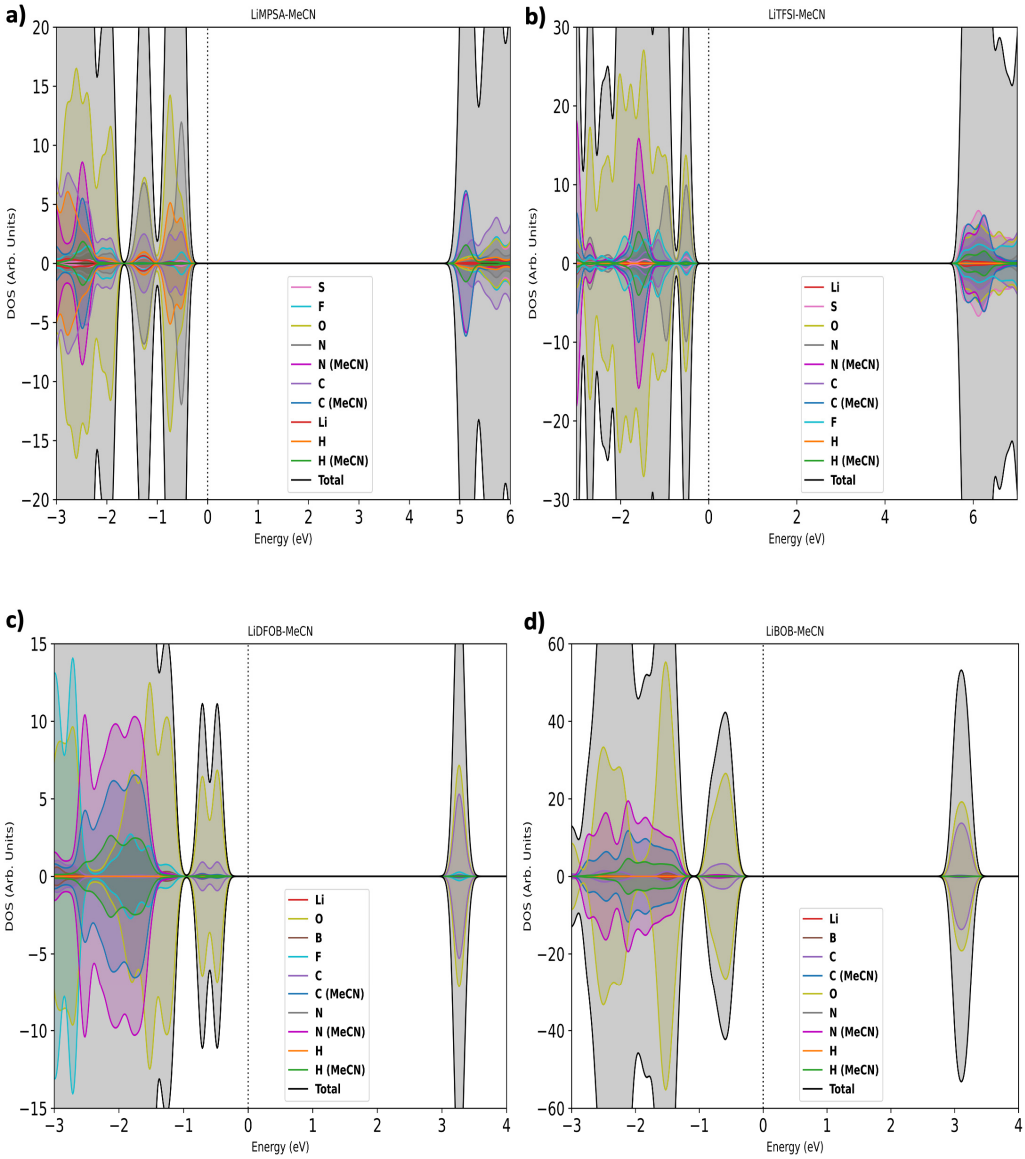

Figure 3. Site-projected electronic density of states (e-DOS) of (**a**) LiMPSA-MeCN, (**b**) LiTFSI-MeCN, (**c**) LiDFOB-MeCN, and (**d**) LiBOB-MeCN. The Fermi level, E_f, is represented by a dotted vertical line and referenced as zero in energy level.

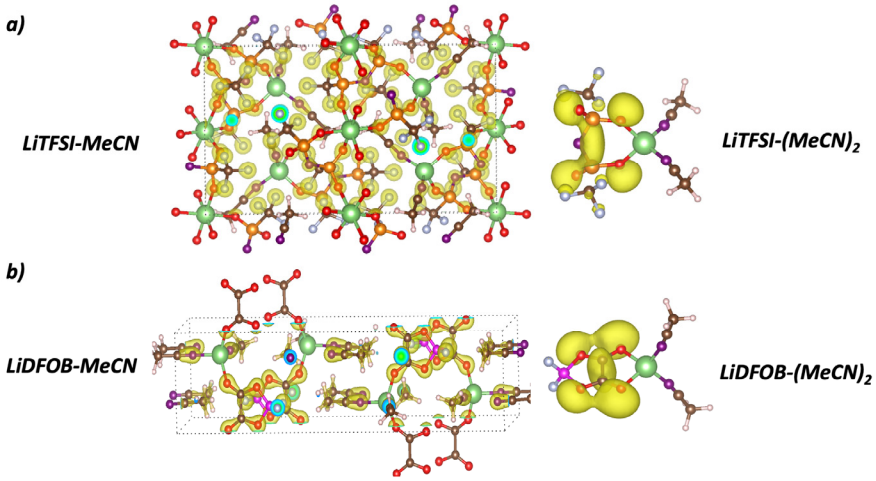

Figure 4. Projected electron density distribution of the top valence band for the solvate crystal (left) and the highest occupied molecular orbital (HOMO) for the salt-MeCN solvate molecule (right): (**a**) LiTFSI-MeCN and LiTFSI-$(MeCN)_2$; (**b**) LiDFOB-MeCN and LiDFOB-$(MeCN)_2$.

3.3. Electrochemical Stability of MeCN and Lithium Salt Molecule

The stability of charged species is important for evaluating the electrochemical stability of a solvent or salt molecule during charge transfer, especially at the charged electrode/electrolyte interfaces. Based on the quantum chemical calculation, all the charged species (anion/cation) of MeCN, LiMPSA, LiTFSI, LiDFOB, and LiBOB are found thermodynamically stable with no imaginary frequencies. Besides redox potentials, it is indispensable to know the adiabatic ionization potential (IP) and electron affinity (EA) of these charged species (Figure 5). Among these systems, all the cationic species are found to be less stable than the neutral species, whereas all the anionic species are found to be more stable than the neutral (with EA ~ 0.18–2.04 eV), except MeCN (with EA ~ −1.0 eV). Therefore, this suggests that the MeCN solvent molecule is not stable during the reduction process.

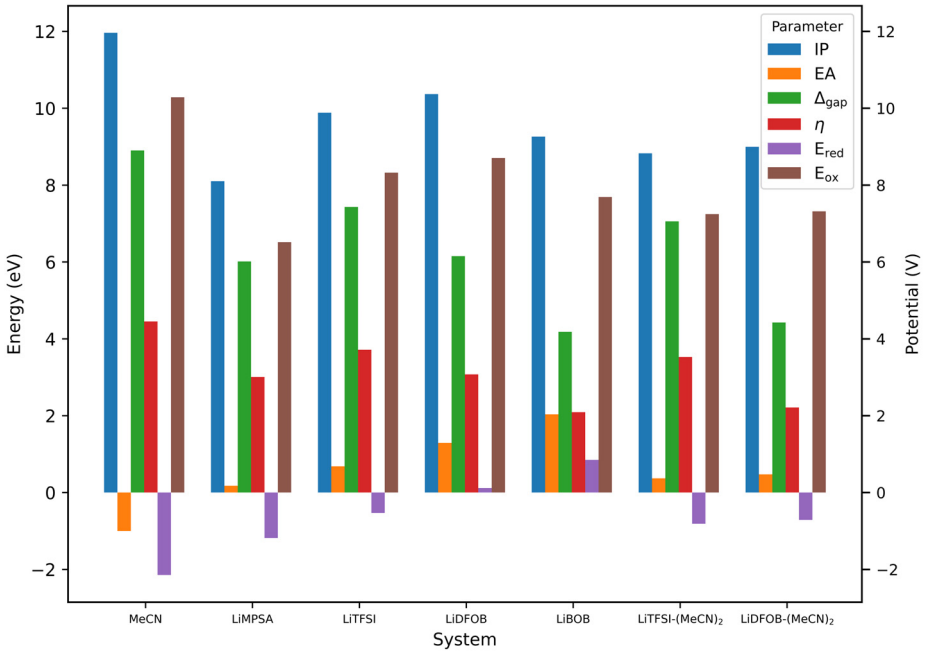

Figure 5. Quantum chemically calculated ionization potential (*IP*, in eV), electronic affinity (*EA*, in eV), HOMO-LUMO gap (Δ_{gap}, in eV), chemical hardness (η, in eV), reduction potential (E_{red}, in V), and oxidation potential (E_{ox}, in V) of MeCN, LiMPSA, LiTFSI, LIDFOB, LiBOB, and the salt-MeCN solvate molecule (LiTFSI-$(MeCN)_2$, LiDFOB-$(MeCN)_2$).

Meanwhile, it is known that the practical applications of high-energy-density Li metal batteries have been limited by anodic instability, which causes serious problems, including low coulombic efficiency and limited cycling performance of high-energy-density Li-ion batteries. To address this challenge, in addition to the development of new solvents or lithium salts, we suggest it is possible to utilize the formation of superconcentrated electrolytes with improved electrochemical stability based on the existing known compounds. For conventional organic solvents such as dimethyl carbonate (DMC), diethyl carbonate (DEC), dimethyl ether (DME), and ethylene carbonate (EC), their inferior stability against Li metal anode hindered the commercialization of high-energy-density Li-ion batteries with lithium metals [38,39]. To address the basic electrochemical stability of MeCN and the lithium salts (i.e., LiTFSI, LiMPSA, LiDFOB, and LiBOB) in this study, the basic differences in stability (accounting for the oxidation and reduction processes) were investigated based on the quantum chemical method (Section 2).

During the redox process, the propensity of solvent and salt molecules to donate or accept an electron in an electrolyte can be measured by its one-electron standard redox potentials (E_{red} and E_{ox}). In this case, MeCN is a polar solvent with inherently high lithium salt solubility capacity; however, it was found that the computed reduction potential of MeCN is large, i.e., $E_{red} \sim -2.15$ V (Figure 5). This suggests that MeCN has poor reductive stability, especially against a lithium metal anode, and therefore a dilute MeCN-based electrolyte might not be practical in high-energy-density Li metal batteries. Compared with MeCN, the lithium salts (i.e., LiTFSI, LiMPSA, LiDFOB, and LiBOB) considered in this work are found to be relatively more stable against lithium metal anodes. It can be found that the calculated E_{red} of these lithium salts increase substantially except LiMPSA ($E_{red} \sim -1.18$ V), which might be attributed to the presence of an organic ether chain in the LiMPSA molecule. Therefore, this suggests that LiMPSA salt might be relatively poor in reductive stability against the lithium metal anode compared with the other lithium salts. Meanwhile, besides reductive stability, a robust electrolyte needs to be resilient against the oxidative process, especially for the development of high-voltage Li-ion batteries [40,41]. To achieve this goal, an oxidation-tolerant electrolyte is deemed necessary. As shown in Figure 5, the trend of computed *IP* is similar to E_{ox}. It was found that the oxidation potential of the MeCN molecule is the highest, i.e., $E_{ox} \sim 10.5$ V. Interestingly, a similar trend was also found among these lithium salts, i.e., $E_{ox} \sim 6.5$–8.7 V, which indicates the inherent high oxidative stability of these compounds compared with conventional carbonate-based electrolytes [40–42].

3.4. Electrochemical Stability and Electronic and Raman Signature of Salt-MeCN Molecular Solvates

Herein, to overcome the MeCN's inherently poor reductive stability while exhibiting remarkably high oxidative stability as an electrolyte in high-voltage, high-density Li-ion batteries with lithium anodes, it is important to investigate the electrochemical stability of salt-MeCN solvate structures. From the LiTFSI-MeCN solvate crystal, it is known that a similar thermodynamically stable LiTFSI-$(MeCN)_2$ solvate structure can be found in ~4 M superconcentrated LiTFSI-MeCN electrolyte [7] as mentioned in Section 3.1.2. As highlighted in Figure 5, high electrochemical stability of the LiTFSI-$(MeCN)_2$ solvate molecule, including its charged counterparts (anion and cation), can be found. From quantum chemical calculations, a high oxidation potential ($E_{ox} \sim 7.2$ V) of LiTFSI-$(MeCN)_2$ was found. In contrast with the unstable anionic MeCN molecule, the anionic LiTFSI-$(MeCN)_2$ solvate molecule was found to be more stable than its neutral counterpart, with $EA \sim 0.37$ eV (Figure 5). Thus, the current finding suggests that a significant increase in the LiTFSI-$(MeCN)_2$ solvate structure in solution will enhance the reductive stability of the ~4 M superconcentrated LiTFSI-MeCN electrolyte in high-voltage Li-ion batteries as reported by Yamada et al. [7]. Interestingly, besides the LiTFSI-$(MeCN)_2$ solvate system, we found that the LiDFOB-MeCN solvate system is promising, and its electrochemical stability

should be comparable to the LiTFSI-MeCN system due to the high electrochemical stability of the LiDFOB-$(MeCN)_2$ solvate molecules (e.g., E_{ox} ~ 7.3 V) (Figure 5).

From Table 1, Figures 3 and 4, it is not difficult to find that the basic electronic properties of salt-MeCN solvate crystals are similar to their constituent salt-MeCN solvate molecules (e.g., LiTFSI-$(MeCN)_2$) in the lattices, which indicates the unique inherent character of molecular solids. At the fundamental molecular level, the high electronic insulating character (E_g ~ 6.7 eV, Table 1) of the LiTFSI-MeCN solvate crystal is supported by a large HOMO-LUMO gap (Δ_{gap}) of separate MeCN ($\Delta_{gap} \sim 8.9\,eV$), LiTFSI ($\Delta_{gap} \sim 7.4\,eV$), and LiTFSI-$(MeCN)_2$ ($\Delta_{gap} \sim 7.1\,eV$) solvate molecules separately (Figure 5) in the lattices. Similarly, this insulating feature is also found in the LiDFOB-MeCN solvate crystal with a smaller band gap (i.e., E_g ~ 3.8 eV) and its constituent LiDFOB-$(MeCN)_2$ solvate molecule ($\Delta_{gap} \sim 4.4$ eV). In general, the high electronic insulating feature guarantees high chemical hardness (η) (Figure 5), which is a measure of the chemical stability of a molecule and compound [43–45]. From DFT calculations [43–45], the chemical hardness of a molecule can be used to quantify the resistance towards electron cloud polarization or deformation of a chemical species, which is defined as: $\eta = \frac{1}{2}\left(\frac{\partial \mu}{\partial N}\right) \sim \frac{1}{2}(\Delta_{gap})$, where μ is the electronic chemical potential and N is the number of electrons. Therefore, this suggests that in addition to electrochemical stability, the presence of a unique salt-MeCN solvate structure might be useful to guarantee the high chemical stability of electrolytes, and this has been proven in a recent study of superconcentrated LiTFSI-MeCN solution (>4 mol dm^{-3}) for fast charging Li-ion batteries by Yamada et al. [7].

To experimentally probe the presence of these electrochemically stable salt-MeCN solvate structures, it is suggested that the Raman spectra are a useful characterization tool [7,11] to capture the signature shift in the vibrational mode upon coordination with Li^+ in solvation. From the simulated Raman spectra in Figure 6, it can be seen that the molecular signature of pristine salt and the MeCN solvent is well-preserved in the salt-MeCN solvate structure. For lithium salts (e.g., LiDFOB and LiTFSI), their Raman signatures are mostly below 2000 cm^{-1}, whereas the rest are attributed to the presence of the MeCN solvent molecule. Compared with reported experimental Raman frequencies [7,11], our predicted values are overestimated in general due to the limitations of DFT electronic structure calculation (e.g., neglect of anharmonicity, approximate treatment of electron correlation, use of finite basis sets) [46]. According to Seo et al. [11], there are 2 Raman signature vibrational bands associated with the MeCN solvent: C-C ($\upsilon \sim 920$ cm^{-1}) and C≡N ($\upsilon \sim 2254$ cm^{-1}) stretching mode shifts can be used as the unique Raman characterization of the MeCN-Li^+ interaction in solvation. However, compared with the DFT-predicted Raman active mode associated with the C-C stretching mode ($\upsilon \sim 930$ cm^{-1}) of MeCN, we found that the C≡N stretching mode ($\upsilon \sim 2365$ cm^{-1}) is more suitable, especially for the probe of charged species of salt-MeCN solvate molecules (Figures 6 and S3) in solution. From the simulated Raman spectra (Figure 6), it was also confirmed that the unique salt-MeCN (e.g., LiTFSI-$(MeCN)_2$) solvate structure in the solvate crystal is equivalent to the superconcentrated LiTFSI-MeCN solution, and this can be shown using the Raman active (Figure 6) C≡N stretching mode of MeCN. For both the LiTFSI-$(MeCN)_2$ and LiDFOB-$(MeCN)_2$ solvate structures, it was found that there is an upshift of ~ 30 cm^{-1} (Figure 6c) and ~ 27 cm^{-1} (Figure 6d) in the C≡N stretching mode when relative to a pristine uncoordinated MeCN solvent molecule ($\upsilon \sim 2365$ cm^{-1}); this indicates a much stronger C≡N stretching bond of MeCN when coordinated with Li^+ in the salt–solvent inner solvation shell, which is qualitatively consistent with reported experimental findings with an upshift of ~30 cm^{-1} [7,11,33] and ~23 cm^{-1} [47], respectively. This unique feature was confirmed in the ~4 M superconcentrated LiTFSI-MeCN electrolyte for the presence of the LiTFSI-$(MeCN)_2$ solvate structure in solution [7]. Interestingly, it was also found that for the presence of anionic or cationic species of salt-MeCN solvate molecules, a smaller upshift with ~18 cm^{-1} was predicted which indicates a weakened C≡N bond relative to a neutral salt-MeCN solvate molecule (Figure 6c,d). For the experimental confirmation of this unique characteristic variation in the C≡N bond during a charged state (i.e., anionic

or cationic state), it therefore should be subjected to future investigation in the future in superconcentrated LiTFSI-MeCN or LiDFOB-MeCN electrolytes.

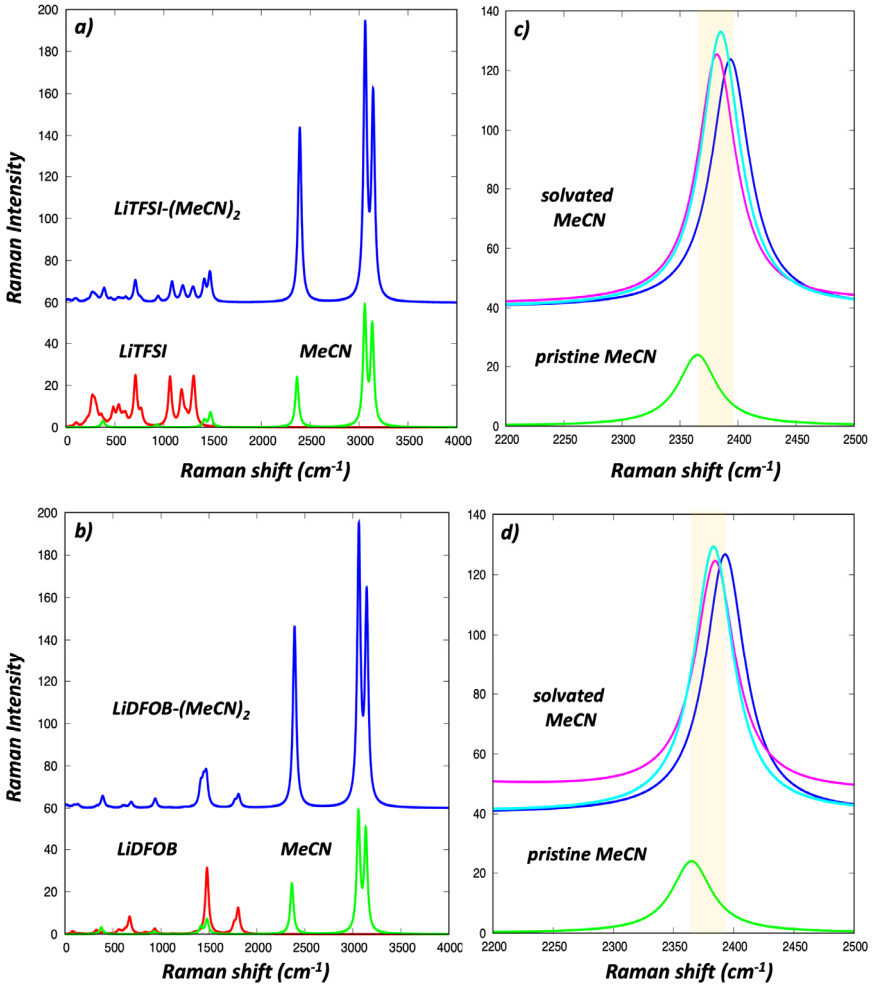

Figure 6. Simulated Raman spectra of (**a**) LiTFSI-$(MeCN)_2$ and (**b**) LiDFOB-$(MeCN)_2$ solvation molecules present in the LiTFSI-MeCN and the LiDFOB-MeCN solvate crystals from Figure 1. The red and green lines are the pristine salt and the MeCN molecule. Graphs (**c**,**d**) show the signature of the C≡N stretching mode (Raman active) that highlights the difference between a pristine MeCN solvent molecule and an Li^+ coordinated MeCN in the (**c**) LiTFSI-$(MeCN)_2$ and the (**d**) LiDFOB-$(MeCN)_2$ solvation structures, which can be observed in solution, especially in superconcentrated MeCN electrolytes. The neutral, anion, and cation MeCN-solvate species are represented by lines in blue, pink, and light blue, respectively.

4. Conclusions

Based on the unique ubiquity of similar solvate structures found in solvate crystals and superconcentrated electrolytes, we performed a systematic study of four reported solvate crystals which consist of different lithium salts (i.e., LiMPSA, LiTFSI, LiDFOB, and LiBOB) solvated by MeCN solvent molecules in different crystalline structures based on first principles calculations. In addition to solvate crystals, basic structure–property relationships of the signature salt-MeCN solvate structures of these systems were analyzed in terms of thermodynamic and electrochemical stability, chemical bonding, and electronic and vibrational properties based on quantum chemical calculations. Among these properties, we found the electrochemical stability and electronic and vibrational properties of these solvate structures are most relevant to lithium battery applications. For these salt-MeCN solvate crystals, the chelate effect of the salt-MeCN solvate complex (e.g., LiTFSI-$(MeCN)_2$, LiDFOB-$(MeCN)_2$) is unique. To understand the basic molecular structures of these salt-

MeCN solvate complexes, their presence can be confirmed by Raman vibrational modes through the unique characteristic variation in the C≡N bond stretching of MeCN molecules in different charged states (e.g., neutral, anion, and cation).

Although the MeCN molecule is highly unstable during the reduction process, it was found that the salt-MeCN solvate molecules (e.g., LiTFSI-$(MeCN)_2$, LiDFOB-$(MeCN)_2$) and their charged counterparts (anions and cations) are both thermodynamically and electrochemically stable. From our calculation, it was found that all these solvate crystals (i.e., E_g ~ 3.8–6.7 eV), including their constituent salt-MeCN solvate molecules ($\Delta_{gap} \sim 4.4 - 7.1$ eV), are highly electronically insulating, which guarantees their electronic and chemical stability. This electronic insulating feature is expected to be similar to their insulating liquid counterpart, which can be pronouncedly represented by a thermodynamically stable stoichiometric mixture of MeCN solvent and salt solvate complex, e.g., ~4 M superconcentrated LiTFSI-MeCN electrolyte (E_g ~ 4 eV), which was confirmed to be a promising electrolyte in lithium batteries. Therefore, in this study, we show that a baseline study in solvate crystals can be useful to help us to understand superconcentrated electrolytes. In addition to the development of new solvents or lithium salts, we suggest it is possible to utilize the formation of superconcentrated electrolytes with improved electrochemical stability based on the existing known or new compounds to facilitate the development of novel electrolyte design in advanced high-energy-density lithium batteries based on lithium metal anodes. However, it is also important to note that even though the salt-MeCN solvate structure was proven to be stable, the MeCN solvent molecules are not guaranteed to always coordinate with Li^+ ions during battery charging and discharging. Therefore, we cannot rule out the possibility that the free MeCN solvent will be released from the solvation structure during the desolvation and deshell processes. Once the free MeCN solvent is released, then the free MeCN molecules in solution might not be stable toward lithium metal anodes. Thus, to maintain robust and stable salt–solvent solvate structures in superconcentrated electrolytes in operating batteries, further detailed investigations remain necessary.

Supplementary Materials: The following supporting information can be downloaded at: https://www.mdpi.com/article/10.3390/en16093700/s1, Table S1: DFT-optimized lattice parameters for salt-MeCN solvate crystals; Figure S1: The crystal structure of MeCN solvent; Figure S2: Site-projected electron density of states (e-DOS) of pristine MeCN, LiMPSA, LiTFSI, LiDFOB, and LiBOB molecules; Figure S3: Quantum chemical method simulated Raman spectra that highlight the difference between a pristine MeCN solvent molecule and a Li^+ coordinated MeCN in the LiTFSI-$(MeCN)_2$ (neutral/anionic/cationic) solvate molecule regarding the C-C stretching mode ($\upsilon \sim 930$ cm^{-1}) of the MeCN molecule.

Author Contributions: Conceptualization, K.C.L.; methodology, J.A.K. and K.C.L.; validation, J.A.K. and K.C.L.; formal analysis, J.A.K. and K.C.L.; investigation, J.A.K. and K.C.L.; resources, K.C.L.; data curation, J.A.K. and K.C.L.; writing—K.C.L.; writing—review and editing, J.A.K. and K.C.L.; visualization, J.A.K. and K.C.L.; supervision, K.C.L.; project administration, K.C.L.; funding acquisition, K.C.L. All authors have read and agreed to the published version of the manuscript.

Funding: This research was funded by the Research Corporation for Science Advancement (RCSA) through a Cottrell Scholar Award (Award# 26829).

Data Availability Statement: Extra data/result can be found in Supporting Information.

Acknowledgments: K.C.L. acknowledges the funding support of the Research Corporation for Science Advancement through the Cottrell Scholar Award and the computing facility supported by NSF MRI program through award number NSF OAC-2117956 and California State University Northridge. We acknowledge the anonymous reviewers' comments in improving this work.

Conflicts of Interest: The authors declare no conflict of interest.

References

1. Grey, C.P.; Hall, D.S. Prospects for lithium-ion batteries and beyond—A 2030 vision. *Nat. Commun.* **2020**, *11*, 6279. [CrossRef] [PubMed]
2. Goodenough, J.B.; Park, K.S. The Li-Ion Rechargeable Battery: A Perspective. *J. Am. Chem. Soc.* **2013**, *135*, 1167–1176. [CrossRef] [PubMed]
3. Kang, X. Electrolytes and Interphases in Li-Ion Batteries and Beyond. *Chem. Rev.* **2014**, *114*, 11503–11618.
4. Riddick, J.A.; Bungh, W.B.; Sakano, T.K. *Organic Solvents: Physical Properties and Methods of Purification*, 4th ed.; Willey: New York, NY, USA, 1986.
5. Rupich, M.W.; Pitts, L.; Abraham, K.M.J. Characterization of Reactions and Products of the Discharge and Forced Overdischarge of Li /SO_2 Cells. *Electrochem. Soc.* **1982**, *129*, 1857–1861. [CrossRef]
6. Jeong, S.-K.; Seo, H.-Y.; Kim, D.-H.; Han, H.-K.; Kim, J.-G.; Lee, Y.B.; Iriyama, Y.; Abe, T.; Ogumi, Z. Suppression of dendritic lithium formation by using concentrated electrolyte solutions. *Electrochem. Commun.* **2008**, *10*, 635–638. [CrossRef]
7. Yamada, Y.; Furukawa, K.; Sodeyama, K.; Kikuchi, K.; Yaegashi, M.; Tateyama, Y.; Yamada, A. Unusual Stability of Acetonitrile-Based Superconcentrated Electrolytes for Fast-Charging Lithium-Ion Batteries. *J. Am. Chem. Soc.* **2014**, *136*, 5039–5046. [CrossRef] [PubMed]
8. Azov, V.A.; Egorova, K.S.; Seitkalieva, M.M.; Kashin, A.S.; Ananikov, V.P. "Solvent-in-Salt" Systems for Design of New Materials in Chemistry, Biology and Energy Research. *Chem. Soc. Rev.* **2018**, *47*, 1250–1284. [CrossRef] [PubMed]
9. Borodin, O.; Self, J.; Persson, K.A.; Wang, C.; Xu, K. Uncharted Waters: Super-Concentrated Electrolytes. *Joule* **2020**, *4*, 69–100. [CrossRef]
10. Yamada, Y.; Yamada, A. Superconcentrated Electrolytes for Lithium Batteries. *J. Electrochem. Soc.* **2015**, *162*, A2406–A2423. [CrossRef]
11. Seo, D.M.; Borodin, O.; Han, S.-D.; Boyle, P.D.; Henderson, W.A. Electrolyte Solvation and Ionic Association II. Acetonitrile-Lithium Salt Mixtures: Highly Dissociated Salts. *J. Electrochem. Soc.* **2012**, *159*, A1489–A1500. [CrossRef]
12. Seo, D.M.; Borodin, O.; Balogh, D.; O'Connell, M.; Ly, Q.; Han, S.-D.; Passerini, S.; Henderson, W.A. Electrolyte Solvation and Ionic Association III. Acetonitrile-Lithium Salt Mixtures: Transport Properties. *J. Electrochem. Soc.* **2013**, *160*, A1061–A1070. [CrossRef]
13. Dillon, R.E.A.; Stern, C.L.; Shriver, D.F. X-ray Structure Determinations of Li[CF3SO2N(CH2)3OCH3] and the Solid Electrolyte [Li⊂12-C-4] [CF3SO2N(CH2)3OCH3]. *Chem. Mater.* **2000**, *12*, 1122–1126. [CrossRef]
14. Seo, D.M.; Boyle, P.D.; Henderson, W.A. Poly[bis(acetonitrile-κN)bis[μ_3-bis(trifluoromethanesulfonyl)imido-κˆ4O,O′:O″:O‴]dilithium]. *Acta Cryst.* **2011**, *E67*, m534.
15. Han, S.-D.; Allen, J.L.; Jonsson, E.; Johansson, P.; McOwen, D.W.; Boyle, P.D.; Henderson, W.A. Solvate Structures and Computational/Spectroscopic Characterization of Lithium Difluoro(oxalate)borate (LiDFOB) Electrolytes. *J. Phys. Chem. C* **2013**, *117*, 5521–5531. [CrossRef]
16. Zavalij, P.Y.; Yang, S.; Whittingham, M.S. Structural Chemistry of new lithium bis(oxalate)-borate solvates. *Acta Cryst.* **2004**, *B60*, 716–724. [CrossRef] [PubMed]
17. Kresse, G.; Furthmüller, J. Efficient Iterative Schemes for Ab Initio Total-Energy Calculations Using a Plane-Wave Basis Set. *Phys. Rev. B* **1996**, *54*, 11169–11186. [CrossRef]
18. Kresse, G.; Furthmüller, J. Efficiency of Ab-Initio Total Energy Calculations for Metals and Semiconductors Using a Plane-Wave Basis Set. *Comput. Mater. Sci.* **1996**, *6*, 15–50. [CrossRef]
19. Blöchl, P.E. Projector Augmented-Wave Method. *Phys. Rev. B* **1994**, *50*, 17953. [CrossRef]
20. Perdew, J.P.; Burke, K.; Ernzerhof, M. Generalized Gradient Approximation Made Simple. *Phys. Rev. Lett.* **1996**, *77*, 3865. [CrossRef]
21. Grimme, S.; Antony, J.; Ehrlich, S.; Krieg, H. A Consistent and Accurate Ab Initio Parametrization of Density Functional Dispersion Correction (Dft-D) for the 94 Elements H-Pu. *J. Chem. Phys.* **2010**, *132*, 154104. [CrossRef]
22. Frisch, M.J.; Trucks, G.W.; Schlegel, H.B.; Scuseria, G.E.; Robb, M.A.; Cheeseman, J.R.; Scalmani, G.; Barone, V.; Petersson, G.A.; Nakatsuji, H.; et al. *Gaussian 16, Revision C.01*; Gaussian, Inc.: Wallingford, CT, USA, 2016.
23. Becke, A.D. Density-functional thermochemistry. III. The role of exact exchange. *J. Chem. Phys.* **1993**, *98*, 5648. [CrossRef]
24. Assary, R.S.; Brushett, F.R.; Curtiss, L.A. Reduction potential predictions of some aromatic nitrogen-containing molecules. *RSC Adv.* **2014**, *4*, 57442–57451. [CrossRef]
25. Marenich, A.V.; Ho, J.; Coote, M.L.; Cramer, C.J.; Truhlar, D.G. Computational electrochemistry: Prediction of liquid-phase reduction potentials. *Phys. Chem. Chem. Phys.* **2014**, *16*, 15068–15106. [PubMed]
26. Lau, K.C.; Kandalam, A.K.; Costales, A.; Pandey, R. Equilibrium geometry and electron detachment energies of anionic Cr_2O_4, Cr_2O_5, and Cr_2O_6 clusters. *Chem. Phys. Lett.* **2004**, *393*, 112–117. [CrossRef]
27. Fu, Y.; Liu, L.; Yu, H.-Z.; Wang, Y.-M.; Guo, Q.-X. Quantum chemical prediction of absolute standard redox potentials of diverse organic molecules and free radicals in acetonitrile. *J. Am. Chem. Soc.* **2005**, *127*, 7227–7234. [CrossRef]
28. Boothroyd, S.; Kerridge, A.; Broo, A.; Buttar, D.; Anwar, J. Why Do Some Molecules Form Hydrates or Solvates? *Cryst. Growth. Des.* **2018**, *18*, 1903–1908. [CrossRef]
29. Grothe, E.; Meekes, H.; Vlieg, E.; ter Horst, J.H.; de Gelder, R. Solvates, Salts, and Cocrystals: A Proposal for a Feasible Classification System. *Cryst. Growth. Des.* **2016**, *16*, 3237–3243. [CrossRef]

30. Schkeryantz, L.; Nguyen, P.; McCulloch, W.D.; Moore, C.E.; Lau, K.C.; Wu, Y. Unusual Melting Trend in an Alkali Asymmetric Sulfonamide Salt Series: Single-Crystal Analysis and Modeling. *Inorg. Chem.* **2021**, *60*, 14679–14686. [CrossRef]
31. Schkeryantz, L.; Nguyen, P.; McCulloch, W.D.; Moore, C.E.; Lau, K.C.; Wu, Y. K^+ Single Cation Ionic Liquids Electrolytes with Low Melting Asymmetric Salt. *J. Phys. Chem. C* **2022**, *126*, 11407–11413. [CrossRef]
32. van de Streek, J. All Series of Multiple Solvates (Including Hydrates) from the Cambridge Structural Database. *CrystEngComm* **2007**, *9*, 350–352. [CrossRef]
33. See, K.A.; Wu, H.-L.; Lau, K.C.; Shin, M.; Cheng, L.; Balasubramanian, M.; Gallagher, K.G.; Curtiss, L.A.; Gewirth, A.A. Effect of Hydrofluoroether Cosolvent Addition on Li Solvation in Acetonitrile-Based Solvate Electrolytes and Its Influence on S Reduction in a Li–S Battery. *ACS Appl. Mater. Interfaces* **2016**, *8*, 34360–34371. [CrossRef] [PubMed]
34. Lau, K.C.; Dunlap, B.I. Lattice dielectric and thermodynamic properties of yttria stabilized zirconia solids. *J. Phys. Condens. Matter* **2009**, *21*, 145402. [CrossRef] [PubMed]
35. Ugata, Y.; Thomas, M.L.; Mandai, T.; Ueno, K.; Dokko, K.; Watanabe, M. Li-Ion Hopping Conduction in Highly Concentrated Lithium Bis (Fluorosulfonyl) Amide/Dinitrile Liquid Electrolytes. *Phys. Chem. Chem. Phys.* **2019**, *21*, 9759–9768. [CrossRef] [PubMed]
36. Camacho-Forero, L.E.; Smith, T.W.; Balbuena, P.B. Effects of High and Low Salt Concentration in Electrolytes at Lithium–Metal Anode Surfaces. *J. Phys. Chem. C* **2016**, *121*, 182–194. [CrossRef]
37. Dokko, K.; Watanabe, D.; Ugata, Y.; Thomas, M.L.; Tsuzuki, S.; Shinoda, W.; Hashimoto, K.; Ueno, K.; Umebayashi, Y.; Watanabe, M. Direct Evidence for Li Ion Hopping Conduction in Highly Concentrated Sulfolane-Based Liquid Electrolytes. *J. Phys. Chem. B* **2018**, *122*, 10736–10745. [CrossRef]
38. Chen, S.; Zheng, J.; Yu, L.; Ren, X.; Engelhard, M.H.; Niu, C.; Lee, H.; Xu, W.; Xiao, J.; Liu, J.; et al. High-Efficiency Lithium Metal Batteries with Fire-Retardant Electrolytes. *Joule* **2018**, *2*, 1548. [CrossRef]
39. Cao, X.; Ren, X.; Zou, L.; Engelhard, M.H.; Huang, W.; Wang, H.; Matthews, B.E.; Lee, H.; Niu, C.; Arey, B.W.; et al. Monolithic solid–electrolyte interphases formed in fluorinated orthoformate-based electrolytes minimize Li depletion and pulverization. *Nat. Energy* **2019**, *4*, 796. [CrossRef]
40. Goodenough, J.B.; Kim, Y. Challenges for Rechargeable Li Batteries. *Chem. Mater.* **2010**, *22*, 587–603. [CrossRef]
41. Manthiram, A. Materials Challenges and Opportunities of Lithium Ion Batteries. *J. Phys. Chem. Lett.* **2011**, *2*, 176–184. [CrossRef]
42. Assary, R.S.; Curtiss, L.A.; Redfern, P.C.; Zhang, Z.; Amine, K. Computational Studies of Polysiloxanes: Oxidation Potentials and Decomposition Reactions. *J. Phys. Chem. C* **2011**, *115*, 12216–12223. [CrossRef]
43. Reed, J.L. Electronegativity: Chemical Hardness I. *J. Phys. Chem. A* **1997**, *101*, 7396–7400. [CrossRef]
44. Parr, R.G.; Pearson, R.G. Absolute hardness: Companion parameter to absolute electronegativity. *J. Am. Chem. Soc.* **1983**, *105*, 7512–7516. [CrossRef]
45. Parr, R.G.; Yang, W. *Density Functional Theory of Atoms and Molecules*, 1st ed.; Oxford University Press: New York, NY, USA, 1989; pp. 70–98.
46. Jiménez-Hoyos, C.A.; Janesko, B.G.; Scuseria, G.E. Evaluation of range-separated hybrid density functionals for the prediction of vibrational frequencies, infrared intensities, and Raman activities. *Phys. Chem. Chem. Phys.* **2008**, *10*, 6621–6629. [CrossRef] [PubMed]
47. Han, S.-D.; Borodin, O.; Allen, J.L.; Seo, D.M.; McOwen, D.W.; Yun, S.-H.; Henderson, W.A. Electrolyte Solvation and Ionic Association IV. Acetonitrile- Difluoro(oxalato)borate (LiDFOB) Mixtures. *J. Electrochem. Soc.* **2013**, *160*, A2100–A2110. [CrossRef]